



Application Research of Hydrogen Production and Water Treatment Based on Photothermal Catalyst Co₃O₄@ZIS

He Jingxian, Liu Jianxia, Gou Hao, Sun Wanjun, Li Na and Wang Kai

EasyChair preprints are intended for rapid dissemination of research results and are integrated with the rest of EasyChair.

November 3, 2024

Application research of hydrogen production and water treatment based on photothermal catalyst $\text{Co}_3\text{O}_4@\text{ZIS}$

He Jing Xian

College of New Energy and Power Engineering
Lanzhou Jiaotong University
Lanzhou, Gansu Province, China
Hejx@lzjtu.edu.cn

Liu Jian Xia*

College of New Energy and Power Engineering
Lanzhou Jiaotong University
Lanzhou, Gansu Province, China
2990702494@qq.com
*Corresponding author

Gou Hao

College of New Energy and Power Engineering
Lanzhou Jiaotong University
Lanzhou, Gansu Province, China
ghao221@lzc.edu.cn

Sun Wan Jun

College of New Energy and Power Engineering
Lanzhou Jiaotong University
Lanzhou, Gansu Province, China
wanjunsun@mail.lzjtu.cn

Li Na

College of New Energy and Power Engineering
Lanzhou Jiaotong University
Lanzhou, Gansu Province, China
Lanzhou, Gansu Province, China
6lina0221@163.com

Wang Kai

College of New Energy and Power Engineering
Lanzhou Jiaotong University
Lanzhou, Gansu Province, China
wangkai163x@126.com

Abstract—In order to solve the double demand problem of shortage of energy and fresh water resources, a photothermal catalyst $\text{Co}_3\text{O}_4@\text{ZIS}$ was prepared by in-situ growth of ZnIn_2S_4 nanosheets on the surface of the photothermal material Co_3O_4 . The photothermal cocatalytic effect promoted the efficiency of photocatalytic decomposition of aquatic hydrogen with an average hydrogen production efficiency of $3186.03 \mu\text{molg}^{-1}\cdot\text{h}^{-1}$. It is about 10 times that of pure ZnIn_2S_4 . Further, the water evaporation experiment was carried out using the photothermal catalyst $\text{Co}_3\text{O}_4@\text{ZIS}$ supported melamine foam. The results showed that the water evaporation rate reached 90.91%, which was 1.2 times higher than that of ZnIn_2S_4 , providing a new idea for realizing the purpose of hydrogen production and water desalination by using photothermal catalytic materials.

Keywords—photothermal catalyst, $\text{Co}_3\text{O}_4@\text{ZIS}$, hydrogen-producing, water treatment style.

I. INTRODUCTION

With the development of economy, the demand for energy increases, leading to the increasing exhaustion of energy and the aggravation of environmental pollution^[1]. Therefore, it is urgent to carry out the transformation of new energy structure and promote the implementation of the process of ‘carbon peaking and carbon neutrality’^[2].

Solar hydrogen production can convert intermittent, fluctuating, low energy flux density solar energy and store it into hydrogen energy chemical energy, the whole process is safe and environmentally friendly, and is expected to achieve large-scale sustainable hydrogen production. Among the various solar hydrogen production methods, the use of photocatalyst to separate H_2 from water is an attractive strategy^[3-6]. In 1972, Honda and Fujijima discovered that photocatalytic TiO_2 electrodes could lead to water decomposition to produce hydrogen, revealing the possibility of photocatalytic decomposition of aquatic hydrogen^[6].

Single photocatalytic technology has defects such as severe electron hole recombination^[7] and low spectral utilization^[8-9], which limit its application. Photothermal cocatalysis can make up for the shortcomings of single photocatalysis^[10]. Domestic and foreign researchers have conducted a large number of studies on photothermal cocatalysis^[11-12], such as: Li et al^[13] proposed a kind of spatial ternary carbon nanospheres, TiO_2 and TiO_{2-x} (denoted as $\text{C}@\text{TiO}_2/\text{TiO}_{2-x}$) egg-shell nanostructures. The carbon nanospheres have good photothermal effects, and the ternary spatial structure of the catalyst accelerates the separation of electrons and holes. Under simulated sunlight, the photothermal catalytic hydrogen production efficiency reached $3667 \mu\text{molg}^{-1}\cdot\text{h}^{-1}$, showing a good hydrogen production efficiency. Zhang Yahai synthesized AB/SCN composites with

AB as the precursor and CuS as the co-catalyst. CuS as the co-catalyst was used to study the catalytic hydrogen production performance of CuS/AB/SCN composites. The results showed that CuS as the co-catalyst could provide more active sites and absorb near infrared light to generate heat, which could increase the temperature of the reaction system. It accelerates the migration of photogenerated carriers and promotes the hydrogen production reduction reaction, and 17% CuS/AB/SCN has the best hydrogen production rate ($4805 \mu\text{mol}\cdot\text{g}^{-1}\cdot\text{h}^{-1}$), showing good hydrogen production cycle stability^[14]. In addition to enhancing hydrogen production efficiency through morphology regulation^[15-17] and element doping^[18-21], heterojunction construction^[22-26] is a widely used strategy.

Photocatalyst ZnIn_2S_4 is an N-type semiconductor with simple synthesis method, narrow band gap and good photocatalytic hydrogen production performance^[27-28], but it has disadvantages such as narrow spectral absorption range and easy recombination of carriers^[29-30], which limits the photocatalytic hydrogen production activity.

As a P-type semiconductor, Co_3O_4 has a narrow band gap, excellent photothermal properties, and can absorb and utilize sunlight in the infrared spectrum region, so it has the potential for photothermal development^[31]. In this paper, photocatalyst ZnIn_2S_4 and photothermal material Co_3O_4 were treated with oil bath to construct a p-n heterojunction photothermal catalyst $\text{Co}_3\text{O}_4@/\text{ZnIn}_2\text{S}_4$. Under simulated sunlight irradiation (optical power density of $100 \text{ mw}/\text{cm}^2$), the H_2 content was calibrated by chromatograph and the hydrogen production efficiency was calculated. Furthermore, the photothermal catalyst $\text{Co}_3\text{O}_4@/\text{ZnIn}_2\text{S}_4$ supported by melamine foam^[32-33] with good water transport was further applied for water treatment research, and the influence of the photothermal catalyst on water evaporation treatment was explored, laying a foundation for the research on the application of photothermal catalyst to promote hydrogen production and water evaporation.

II. EXPERIMENTAL PART

A. Materials

All analytical grade chemicals are used as received. Zinc chloride (ZnCl_2 , 98%), cobalt nitrate ($\text{Co}(\text{NO}_3)_2$, 99%) from Shanghai Zhanyun Chemical Co. LTD., thioacetamide (TAA, 99%) from Tianjin Guangfu Technology Co. LTD., anhydrous sodium sulfate (Na_2SO_4 , 99%) from Sichuan Xilong Science Co. LTD., glycerin (99%), hydrochloric acid (HCl, 36-38%), ethanol (99.7%) and triethanolamine (TEOA, 98%) were purchased from Tianjin Damao Reagent Factory. Indium trichloride tetrahydrate ($\text{InCl}_3\cdot 4\text{H}_2\text{O}$, 99%), 2-methylimidazole (98%) and glycerol ($\text{C}_3\text{H}_8\text{O}_3$, 99%) were purchased from Shanghai Aladdin Industrial Co. LTD.

B. Preparation method

Co_3O_4 was prepared by static centrifugation and high temperature calcination. 6 mmol cobalt nitrate and 24 mmol dimethylimidazole were added to 100 ml methanol and stirred for 30 min respectively. After mixing and stirring for 30 min, the blue particles were collected by centrifugation, washed alternately with methanol and ethanol, and dried at 60°C for 24 h in a vacuum drying oven to form hexagonal ZIF-67 nanoparticles. Then, the ZIF-67 nanoparticles were heated in a

tube furnace at a rate of $1^\circ\text{C}/\text{min}$, and were calcined under vacuum at 550°C for 2 h to form sunken Co_3O_4 nanoparticles.

$\text{Co}_3\text{O}_4@/\text{ZIS}$ was synthesized by water bath centrifugation method^[34]. 96ml distilled water was added into a single-neck flask and the pH value was adjusted with HCl solution (3 mol/L) to 2.5. Then 24 ml glycerol and 10mg Co_3O_4 were added. ZnCl_2 (136.3 mg), $\text{C}_2\text{H}_5\text{NS}$ (293.24 mg) and $\text{InCl}_3\cdot 4\text{H}_2\text{O}$ (293.24 mg) were added to the mixture. After homogenization by ultrasound, the mixture was stirred in an oil bath and kept at 80°C for 2 h under circulating condensation condition. The mixture was collected after cooling and then centrifuged alternately with anhydrous ethanol and water. Then the products were collected after 12 h in a vacuum drying oven at 60°C $\text{Co}_3\text{O}_4@/\text{ZIS}$. In the above mixed solution, ZnIn_2S_4 nanoparticles can be obtained after heating in the oil bath and centrifuging drying without adding Co_3O_4 .document.

C. Material Characterization

The crystallinity of the sample was determined by X-ray diffraction (XRD) (Bruker D8 Advance; Cu target) was tested at a sweep speed of $1^\circ/\text{min}$. The field emission electron microscope (Gemini SEM 500) was used to measure the morphology of the samples under high vacuum. The surface chemical valence and charge transfer of the photocatalyst were measured using X-ray photoelectron spectroscopy (XPS) (PHI 5000 VersaprobeIII, contaminated carbon (284.8 eV) as reference). The spectroscopic absorption range of the photocatalyst was tested using a UV-vis-NIR with BaSO_4 as a reference (UH 4150, Japan). The photoluminescence (PL) spectra of the photocatalyst were tested using a fluorescence spectrometer (F-7000, Japan).

D. Performance Characterization

The hydrogen production performance of the photothermal catalyst was tested using a Fuli gas chromatograph. Xenon lamp source equipped with AM1.5G filter was used to keep the vacuum in the bottle after the replacement gas. The light was measured every 1h, and the hydrogen production efficiency was calculated by a cycle of 4 h. The transient photocurrent, electrochemical impedance (EIS) and Mott-Schottky curves of the photothermal catalyst were recorded on the electrochemical workstation (Chen Hua). In a three-electrode system, 0.5 mol/L Na_2SO_4 solution was selected for the electrolyte, Ag/AgCl was selected for the reference electrode, and Pt sheet electrode was used for the electrode. After ultrasonic mixing of photocatalyst and ethanol solution, droplets were added to the FTO substrate as the working electrode.

III. RESULTS AND DISCUSSIONS

A. Characterization of photothermal catalysts

As shown in the figure 1, The morphology of samples ZIF-67 (Figure 1 (a)), Co_3O_4 (Figure 1 (b)), ZnIn_2S_4 (Figure 1 (c)) and $\text{Co}_3\text{O}_4@/\text{ZIS}$ (Figure 1 (d)) were characterized by scanning electron microscopy (SEM). ZIF-67 showed a hexagonal structure after precipitation in water bath, which was consistent with the structural characteristics of ZIF-67^[35]. The Co_3O_4 formed after high-temperature calcination of ZIF-67 has the characteristic of being concave around the middle^[36], which may be due to the removal of the sides of the regular hexagonal body

of ZIF-67 after high-temperature annealing treatment. Figure 1 (c) shows the nanoflower-like structure of ZnIn_2S_4 , which is composed of stacked nanosheets^[37]. In Figure 1, the nanoflower-like structure of Co_3O_4 @ZIS can be clearly observed, while Co_3O_4 is not exposed on the surface of the nanoflower, which is speculated to be due to the tight encapsulation of Co_3O_4 by the hollow nanostructured structure of ZIS. Further Mapping tests were carried out for each element Co_3O_4 @ZIS (Figure 1 (e-i)). It can be seen from the figure that Zn, In, S and Co are uniformly dispersed, and the signal of Co is relatively weak, which is consistent with the preparation expectation.

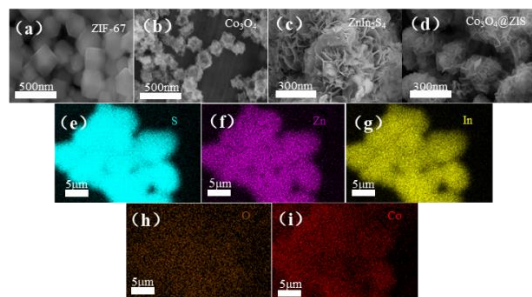


Figure 1. SEM spectra of all samples: (a) ZIF-67. (b) Co_3O_4 . (c) ZnIn_2S_4 . (d) Co_3O_4 @ZIS. (e-i) The mapping image of Co_3O_4 @ZIS.

energy dispersive X-ray spectroscopy (EDS) test revealed the peak locations of Co_3O_4 @ZIS elements. As shown in Figure 2 and observed that there were no hetero-peaks in the spectra, indicating that the photothermal catalyst was prepared with high purity, and the content of Co was detected, indicating that Co_3O_4 @ZIS heterojunction was successfully constructed.

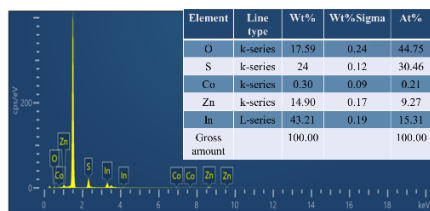


Figure 2. EDS energy spectrum.

The crystal structure and phase composition of the synthesized samples were measured by X-ray diffractometer (XRD). Four strong characteristic diffraction peaks appeared at 21.6° , 27.74° , 30.14° and 47.41° for ZIS and Co_3O_4 @ZIS, As shown in Figure 3 (a), Corresponding to the (006), (102), (104), (110) lattice planes (PDF#04-009-4783) of the hexagonal phase ZIS, respectively, similar to the association reported by ZnIn_2S_4 ^[38]. As shown in Figure 3 (b), Co_3O_4 appears a strong characteristic diffraction peak at 37.15° , corresponding to the (400) lattice surface of the cubic phase Co_3O_4 (PDF#97-005-6123)^[39]. The weak characteristic diffraction peak corresponding to the Co_3O_4 (400) crystal plane is observed in the XRD pattern of the Co_3O_4 @ZIS composite sample. It is speculated that the weak characteristic diffraction peak may be due to the relatively small content of Co_3O_4 . It also indicates the smooth construction of Co_3O_4 @ZIS heterojunction.

X-ray photoelectron spectroscopy (XPS) of samples ZIS, Co_3O_4 @ZIS and Co_3O_4 can be used to analyze the chemical states of the elements on the surface of the prepared samples. By

comparing the Zn 2p, In 3d and S 2p spectra of ZIS and Co_3O_4 @ZIS, Figure 4 (a-c), it can be found that the Zn 2p and In 3d peaks of Co_3O_4 @ZIS move in the direction of high binding energy, and the S 2p peaks of Co_3O_4 @ZIS move in the direction of low binding energy. This indicates that there is an electron gain and loss interaction between ZIS and Co_3O_4 , indicating the smooth construction of heterojunctions, which is consistent with literature^[40-45].

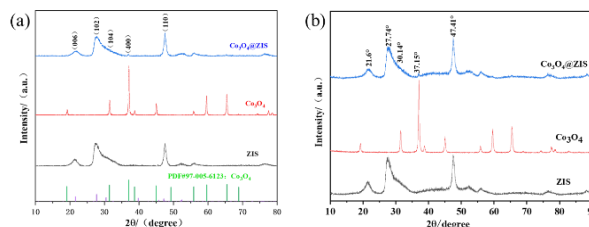


Figure 3. (a) XRD patterns of ZIS, Co_3O_4 and Co_3O_4 @ZIS composites (crystal face). (b) XRD patterns of ZIS, Co_3O_4 and Co_3O_4 @ZIS composites (Angle).

However, the valence peak of Co is not detected in the energy spectrum of Co_3O_4 @ZIS, such as Figure 4 (d), which may be due to the nanostructured structure of ZIS, and Co_3O_4 is tightly wrapped by ZIS after composite. X-ray can only detect the valence peak of the compound on the surface, so the valence peak of Co cannot be detected.

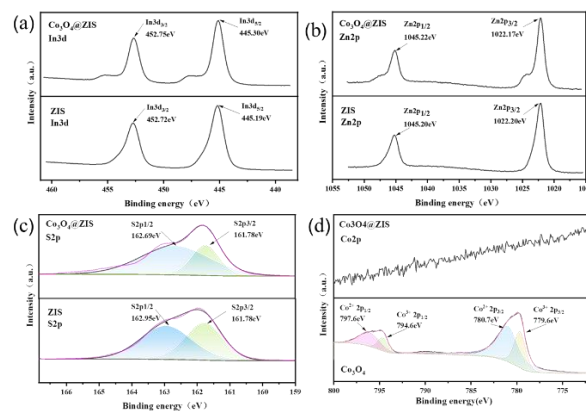


Figure 4. XPS spectra of Zn 2p (a), In 3d (b), S 2p (c) for ZIS and Co_3O_4 @ZIS. XPS spectra of Co 2p for Co_3O_4 @ZIS and Co_3O_4 (d).

B. Analysis of hydrogen production performance of photothermal cocatalysis

As is shown in Figure 5 (a), The spectral absorption range was tested by the UV-visible near-infrared spectrometer (UV-Vis-Nir). ZIS responded to visible light and showed a maximum absorption edge at about 500 nm, with almost no light absorption in the near-infrared region. Co_3O_4 showed a wide and strong light absorption capacity from ultraviolet to near-infrared, with the potential to produce photothermal effects. After combining with Co_3O_4 , the spectral absorption range and absorption intensity of Co_3O_4 @ZIS obviously increase, indicating that it has good spectral utilization ability.

The gas content was tested every 1h under a hernia light source with optical power density of 100 mw/cm^2 , and H_2 content was calibrated by gas chromatograph. After conversion, it was concluded that after the combination of photocatalyst ZIS

and Co_3O_4 , the maximum hydrogen production efficiency of $\text{Co}_3\text{O}_4@ZIS$ composite sample could reach $3186.03 \mu\text{mol g}^{-1}\cdot\text{h}^{-1}$. About 10 times the hydrogen production rate of ZIS, exam. Figure 5 (b).

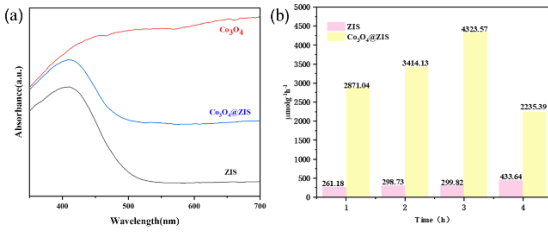


Figure 5. (a) UV-vis-NIR absorption spectra of ZIS, Co_3O_4 and $\text{Co}_3\text{O}_4@ZIS$ composites with different contents of Co_3O_4 . (b) Hydrogen production efficiency of ZIS and $\text{Co}_3\text{O}_4@ZIS$.

C. Mechanism analysis of photothermal cocatalysis

Photoluminescence spectroscopy (PL) explores the carrier separation efficiency of photocatalyst. Such as Figure 6 (a), pure ZIS has the strongest PL peak at about 500 nm, and the higher the PL peak, the easier the carrier recombination is, because the carrier transitions between band gaps, resulting in charge recombination. Co_3O_4 has the lowest PL peak, indicating that charge recombination is not easy to occur. In $\text{Co}_3\text{O}_4@ZIS$ composite, PL peak is obviously weakened due to the addition of Co_3O_4 , indicating that the addition of Co_3O_4 effectively inhibits the photogenerated carrier recombination, and the carrier separation efficiency is gradually improved. The electrochemical impedance (EIS) represents the resistance of charge in the process of carrier migration. The smaller the impedance radius, the lower the corresponding resistance, the higher the carrier migration efficiency. It can be shown from the figure 6 (b) that ZIS has the largest impedance radius, while $\text{Co}_3\text{O}_4@ZIS$ has the smallest impedance radius, indicating that the introduction of Co_3O_4 effectively accelerates the carrier migration. It speeds up hydrogen production. The transient photocurrent and EIS have the same characterization significance. In $\text{Co}_3\text{O}_4@ZIS$, such as Figure 6 (c), the transient photocurrent response is the largest, indicating that $\text{Co}_3\text{O}_4@ZIS$ can effectively accelerate the carrier migration, thus improving the catalytic performance.

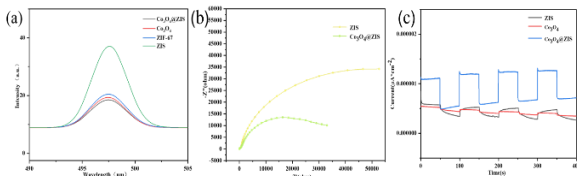


Figure 6. (a) PL spectrum of ZIS, Co_3O_4 , $\text{Co}_3\text{O}_4@ZIS$; (b) EIS diagram of ZIS, $\text{Co}_3\text{O}_4@ZIS$; (c) transient photocurrent curve of ZIS, Co_3O_4 , $\text{Co}_3\text{O}_4@ZIS$.

The Mott-Schottky curve can be used to calculate the type of semiconductor. From the positive and negative slope of the tangent slope of the Mott-Schottky curve of ZIS and Co_3O_4 , such as Figure 7 (a-b), it can be determined that ZIS is an N-type semiconductor and Co_3O_4 is a P-type semiconductor.

When the N-type semiconductor ZIS and the P-type semiconductor Co_3O_4 are in close contact, p-n heterojunction will be formed between them. Due to the diffusion of electrons

and holes, two space charge regions are established at the interface of the p-n junction and an electric field in the space charge region is formed. The presence of the built-in electric field at the interface of the p-n heterojunction can drive the rapid separation and migration of carriers, thus improving the efficiency of carrier separation and migration. The formation principle of p-n junction is shown in Figure 8.

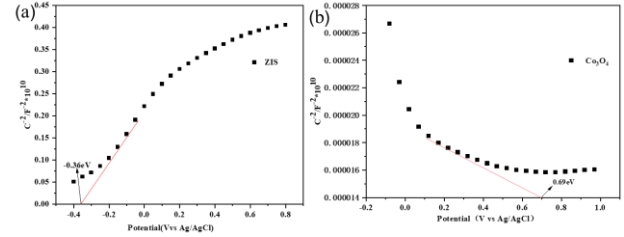


Figure 7. Mott-Schottky curve: (a) ZIS. (b) Co_3O_4 .

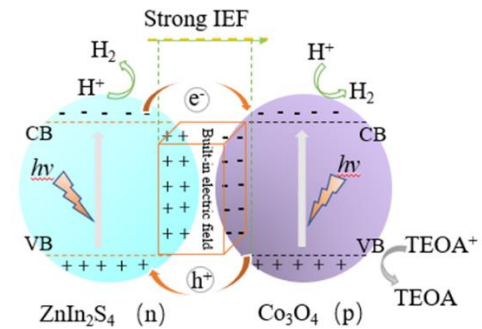


Figure 8. The proposed of charge transfers for $\text{Co}_3\text{O}_4@ZIS$ under light irradiation.

In summary, it can be inferred that the improvement of $\text{Co}_3\text{O}_4@ZIS$ photothermal catalyst performance is largely due to the addition of Co_3O_4 , which significantly improves the carrier separation and migration rate, inhibits the carrier recombination, and thus improves the hydrogen production performance.

IV. WATER TREATMENT APPLICATION RESEARCH

Melamine foam has the advantages of cheap, easy to obtain, reusable, using melamine foam as a base can play a good role in water transport, is a potential water evaporation material. The photothermal co-catalyst $\text{Co}_3\text{O}_4@ZIS$ was used to load melamine foam, and the water evaporation experiment was carried out by xenon lamp on the weighing balance at the power density of 100 mw/cm^2 . The evaporation efficiency of the effluent was calculated by recording the change of water quality, and then the surface temperature of the evaporator was recorded with the aid of an infrared camera.

As is shown the Figure 9(a-b), It can be intuitively understood from the data that the evaporation efficiency of the melamine foam coated with $\text{Co}_3\text{O}_4@ZIS$ reached 90.91% due to its better water transport characteristics, which was 1.2 times that of pure water. Moreover, the surface temperature of the melamine foam coated with $\text{Co}_3\text{O}_4@ZIS$ has a greater change, exam. Figure 9(c-d), and the temperature can rise from the initial 25.8°C to 53.9°C within one hour, which once again proves that $\text{Co}_3\text{O}_4@ZIS$ has better photothermal effect. This theory lays a foundation for improving water pollution and alleviating the

shortage of fresh water resources by promoting water evaporation.

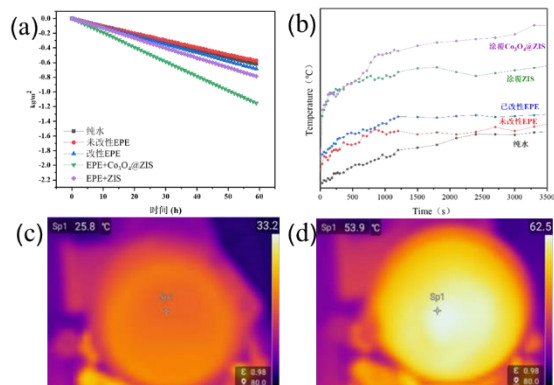


Figure 9. (a) Water evaporation diagram. (b) Temperature rise diagram. (c-d) $\text{Co}_3\text{O}_4@\text{ZIS}$ Temperature change for 1h after loading melamine foam.

V. CONCLUSION

In general, by combining the photothermal effect of Co_3O_4 with photocatalyst ZnIn_2S_4 , the photothermal catalytic material $\text{Co}_3\text{O}_4@\text{ZIS}$ prepared by us has overcome the problems of easy electron hole recombination and low spectral utilization of ZIS itself. On the contrary, the close connection of the internal electric field between $\text{Co}_3\text{O}_4@\text{ZIS}$ inhibits the electron hole recombination, thus enlarging the spectral absorption range. Moreover, the hydrogen production efficiency of the photothermal catalytic material $\text{Co}_3\text{O}_4@\text{ZIS}$ increases to $3186.03 \mu\text{mol}\cdot\text{g}^{-1}\cdot\text{h}^{-1}$, which is about 10 times higher than that of the ZIS photocatalyst. At the same time, the photothermal catalyst $\text{Co}_3\text{O}_4@\text{ZIS}$ was loaded on the melamine foam. Through the water evaporation experiment, it was found that the photothermal effect of the photothermal catalyst $\text{Co}_3\text{O}_4@\text{ZIS}$ was the best, and the water evaporation rate was up to 90.91%. This discovery provided a new solution for solving the problem of fresh water shortage and water pollution, and had good development potential.

ACKNOWLEDGMENT

We are grateful for the Open Fund of Key Laboratory of Eco functional Polymer Materials of the Ministry of Education under Grant No. KF-22-05, the Gansu Province University Industry Support Plan Project (2024CYZC-56), Lanzhou Science and Technology Plan Project (2024-3-2), the Gansu Provincial Department of Education: University teachers innovation fund project (2024A-043), the Young Science Research Foundation of Lanzhou Jiaotong University (2023025), Foundation of Key Laboratory of Solar Power System Engineering (2023SPKL01).

REFERENCES

- [1] M. Salehi, "Global water shortage and potable water safety: Today's concern and tomorrow's crisis", *Environment International*, vol. 158, pp. 106936, January 2022.
- [2] Y.L. Liu, X. Guo, W.T. Dai, "China's carbon emission status and emission reduction path under the vision of "carbon neutrality"", *Journal of Earth Environment*, vol. 14(06), pp. 683-700, 2023.
- [3] T. Hisatomi, K. Domen, "Reaction systems for solar hydrogen production via water splitting with particulate semiconductor photocatalysts". *Nature Catalysis*, vol. 2, pp. 387-399, 2019.
- [4] A. Fujishima, K. Honda, "Electrochemical photolysis of water at a semiconductor electrode". *Nature*, vol. 238(5358), pp. 37-38, 1972.
- [5] H. Nishiyama, T. Yamada, M. Nakabayashi, "Photocatalytic solar hydrogen production from water on a 100 m² scale". *Nature*, vol. 598, pp. 304-307, 2021.
- [6] T. Hisatomi, K. Domen, "Reaction systems for solar hydrogen production via water splitting with particulate semiconductor photocatalysts". *Nature Catalysis*, vol. 2, pp. 387-399, 2019.
- [7] C. Acar, I. Dincer, G.F. Naterer, "Review of photocatalytic water-splitting methods for sustainable hydrogen production", *Int. J. Energy Res*, vol. 40, pp. 1449-1473, 2016.
- [8] T. Takata, K. Domen, "Particulate photocatalysts for water splitting: recent advances and future prospects", *ACS Energy Lett*, vol. 4, pp. 542-549, 2019.
- [9] L. Yuan, C. Han, M.Q. Yang, Y.J. Xu, "Photocatalytic water splitting for solar hydrogen generation: fundamentals and recent advancements", *Int. Rev. Phys.Chem.* vol. 35, pp. 1-36, 2016.
- [10] J.X. He, J.X. Liu, H. Gou, "Progress and discussion on photothermal catalytic hydrogen production", *Materials Review*, pp. 1-18, Oct 2024, in press.
- [11] M.Y. Qi, M. Conte, M. Anpo, Z.R. Tang, Y.J. Xu, "Cooperative Coupling of Oxidative Organic Synthesis and Hydrogen Production over Semiconductor-Based Photocatalysts", *Chem. Rev.* vol. 121, pp. 13051-13085, 2021.
- [12] J.R. Wang, K. He, Ch.L. Li, "Research progress of hydrogen production by solar photothermal catalysis", *Industrial Catalysis*, vol. 32, pp. 20-25, 2024.
- [13] Y. Li., J. Xue, Q. Shen, "Construction of a ternary spatial junction in yolk-shell nanoreactor for efficient photothermal catalytic hydrogen generation", *Chemical Engineering Journal*, vol. 423, pp. 130188, 2021.
- [14] Y.H. Zhang, "Design and Synthesis of Graphitic Carbon Nitride-based Composite Materials and Their Study on Photocatalytic and Photothermal Catalytic Hydrogen Production Performance. Master's thesis", Jiangsu University, China, 2023.
- [15] X.L. Li, N.Li, Y.Q. Gao, "Design and applications of hollowstructured nanomaterials for photocatalytic H₂ evolution and CO₂ reduction". *Chinese Journal of Catalysis*, vol. 43(3), pp. 679-707, 2022.
- [16] Y.Z. Wei, F.F. You, D.C. Zhao, "Heterogeneous hollow multishelled structures with amorphous-crystalline outer-shells for sequential photoreduction of CO₂", *Angewandte Chemie International Edition*, vol. 61(49), pp. e202212049, 2022.
- [17] J.Y. Wang, M. Yang, D. Wang, "Progress and perspectives of hollow multishelled structures", *Chinese*

- Journal of Chemistry, vol. 40(10), pp. 1190-1203, 2022.
- [18] J.Q. Xu, Z.Y. Ju, W. Zhang, "Efficient infrared-light-driven CO₂ reduction over ultrathin metallic Ni-doped CoS₂ nanosheets", *Angewandte Chemie International Edition*, vol. 60(16), pp. 8705-8709, 2021.
- [19] L. He, W. Y. Zhang, K. Zhao, "Core-shell Cu@Cu₂O nanoparticles embedded in 3D honeycomb-like N-doped graphitic carbon for photocatalytic CO₂ reduction", *Journal of Materials Chemistry A*, vol. 10(9), pp. 4758-4769, 2022.
- [20] H.B. Yu, J.H. Huang, L.B. Jiang, "In situ construction of Sndoped structurally compatible heterojunction with enhanced interfacial electric field for photocatalytic pollutants removal and CO₂ reduction", *Applied Catalysis B: Environmental*, vol. 298, pp. 120618, 2021.
- [21] X.T. Mu, L.H. Chen, N.N. Qu, J.L. Yu, X.Q. Jiang, Ch.H. Xiao, X.P. Luo, Q. Hasi, "MXene/polypyrrole coated melamine-foam for efficient interfacial evaporation and photodegradation", *Journal of Colloid and Interface Science*, vol. 636, pp. 291-304, 2023.
- [22] B.Q. Xia, B.W. He, J.J. Zhang, "TiO₂/FePS₃ S-scheme heterojunction for greatly raised photocatalytic hydrogen evolution", *Advanced Energy Materials*, vol. 12(46), pp. 2201449, 2022.
- [23] Zh.H. Xu, H.J. Li, Y. Gao, "Preparation and visible light catalytic performance of In₂O₃/Ag : ZnIn₂S₄ "Type II" heterogeneous materials", *Journal of Chemical Engineering*, vol. 73(8), pp. 3625-3635, 2022.
- [24] Z.H. Xu, H.J. Li, Y. Gao, "Preparation of In₂O₃/Ag : ZnIn₂S₄ "Type II" heterogeneous structure materials for visible light catalysis", *CIESC Journal*, vol. 73(8), pp. 3625-3635, 2022.
- [25] H.M. Li, Q.Q. Shen, H. Zhang, "Oxygen vacancy-mediated WO₃ phase junction to steering photogenerated charge separation for enhanced water splitting", *Journal of Advanced Ceramics*, vol. 11(12), pp. 1873-1888, 2022.
- [26] Li. Wen, X.P. Qi, H. Yang, H.H. Jiang, and T.X. Liang, "MoS₂ in-situ growth on melamine foam for hydrogen evolution", *Functional Materials Letters*, vol. 12(04), pp. 1950044, 2019.
- [27] E. Zhang, Q. Zhu, J. Huang, J. Liu, G. Tan, C. Sun, T. Li, S. Liu, Y. Li, H. Wang, X. Wan, Z. Wen, F. Fan, J. Zhang, K. Ariga, "Visually resolving the direct Z-scheme heterojunction in CdS@ZnIn₂S₄ hollow cubes for photocatalytic evolution of H₂ and H₂O₂ from pure water", *Appl Catal B*, vol. 293, pp. 120213, 2021.
- [28] C. Liu, Q. Zhang, Z. Zou, "Recent advances in designing ZnIn₂S₄-based heterostructured photocatalysts for hydrogen evolution", *J. Mater. Sci. Technol*, vol. 139, pp. 167-188, 2023.
- [29] J. Wang, S. Sun, R. Zhou, Y. Li, Z. He, H. Ding, D. Chen, W. Ao, "A review: synthesis, modification and photocatalytic applications of ZnIn₂S₄", *J. Mater. Sci. Technol*, vol. 78, pp. 1-19, 2021.
- [30] Y. Kumar, R. Kumar, P. Raizada, A.A.P. Khan, Q.V. Le, P. Singh, V.H. Nguyen, "Novel Z-Scheme ZnIn₂S₄-based photocatalysts for solar-driven environmental and energy applications: progress and perspectives", *J. Mater. Sci. Technol*, vol. 87, pp. 234-257, 2021.
- [31] L.B. Gao, Q. Zhang, J.Y. Li, "The cobalt oxide photocatalytic hydrogen or oxygen research progress". *Journal of modern chemical industry*, vol. 10, pp. 68-71, 2014.
- [32] C. Chang, M. Liu, L. Li, "Salt-rejecting rGO-coated melamine foams for high-efficiency solar desalination", *Journal of Materials Research*, vol. 37, pp. 294-303, 2022.
- [33] J. Wang, W.B. Yang, F.F. He, Ch.Q. Xie, J.H. Fan, J.Y. Wu, K. Zhang, "Superhydrophobic Melamine-formaldehyde Foam Prepared by In-situ Coprecipitation", *Chemistry Letters*, vol. 47, pp. 414-416, April 2018.
- [34] Sh.Y. Zhang, G.X. Zhang, Sh.Zh. Wu, "Fabrication of Co₃O₄@ZnIn₂S₄ for photocatalytic hydrogen evolution: Insights into the synergistic mechanism of photothermal effect and heterojunction", *Journal of Colloid and Interface*, vol. 650, pp. 1974-1982, 2023.
- [35] R. Gallegos-Monterrosa, R.O. Mendiola, Y. Nuñez, "Antibacterial and antibiofilm activities of ZIF-67". *J Antibiot*, vol. 76, pp. 603-612, 2023.
- [36] G.T. Chai, D. Du, Ch. Wang, Ch.H. Zhang, L. Cardenas, N. Bion, Y.L. Guo, S. Gil, G.F. Anne, "Spinel Co₃O₄ oxides-support synergistic effect on catalytic oxidation of toluene", *Applied Catalysis A: General*, vol. 614, pp. 118044, 2021.
- [37] Ch. Chen, W.Q. Hou, Y.M. Xu, "Significantly increased production of H₂ on ZnIn₂S₄ under visible light through co-deposited CoWO₄ and Co₃O₄", *Applied Catalysis B: Environmental*, vol. 316, pp. 121676, 2022.
- [38] X. Zhang, S. Ding, X. Luo, C. Huang, T. Dong, Y. Yang, N. Liu, J. Hu, "Engineering amorphous red phosphorus onto ZnIn₂S₄ hollow microspheres with enhanced photocatalytic activity", *Mater. Lett*, vol. 232, pp. 78-81, 2018.
- [39] E. Zhang, Q. Zhu, J. Huang, J. Liu, G. Tan, C. Sun, T. Li, S. Liu, Y. Li, H. Wang, "Visually resolving the direct Z-scheme heterojunction in CdS@ZnIn₂S₄ hollow cubes for photocatalytic evolution of H₂ and H₂O₂ from pure water", *Appl. Catal. B-Environ*, vol. 293, pp. 120213, 2021.
- [40] D.L. Legrand, H.W. Nesbitt, G.M. Bancroft, "X-ray photoelectron spectroscopic study of a pristine millerite (NiS) surface and the effect of air and water oxidation", *Am. Mineral*, pp. 1256-1265, 1998.
- [41] G. Deroubaix, P. Marcus, "X-ray photoelectron spectroscopy analysis of copper and zinc oxides and sulphides", *Surf. Interface Anal*, vol. 18, pp. 39-46, 1992.
- [42] K. Laajalehto, I. Kartio, P. Nowak, "XPS study of clean metal sulfide surfaces", *Appl. Surf. Sci*, vol. 81, pp. 11-15, 1994.
- [43] S.H. Yu, L. Shu, Y.S. Wu, J. Yang, Y. Xie, Y.T. Qian, "Organothermal synthesis and characterization of nanocrystalline β-Indium Sulfide", *J. Am. Ceram. Soc*, vol. 82, pp. 457-460, 1999.
- [44] C. Chen, J. Zhao, M. Chen, W. Hou, Y. Xu, "In situ photodeposition of cobalt nanoparticles onto ZnIn₂S₄ enhancing H₂ production under visible light", *Mol. Catal*,

vol. 515, pp. 111930, 2021.

[45] L.J. Garces, B. Hincapie, R. Zerger, S.L. Suib, “The effect of temperature and support on the reduction of cobalt

oxide: an in situ x-ray diffraction study”, *J. Phys. Chem. C*, vol. 119, pp. 5484–5490, 2015.

Authors' background

Your Name	Title*	Research Field	Personal website
Liu Jianxia	master student	Solar interface photothermal catalytic hydrogen production	none

*This form helps us to understand your paper better, **the form itself will not be published**. Please make sure that you have deleted this form in your final paper after acceptance.

*Title can be chosen from: master student, Phd candidate, assistant professor, lecture, senior lecture, associate professor, full professor